

Efficient weighted-ensemble network simulations of the SIS model of epidemics

Elad Korngut¹, Ohad Vilk^{1,2} and Michael Assaf¹

¹*Racah Institute of Physics, Hebrew University of Jerusalem, Jerusalem 91904, Israel*

²*Movement Ecology Lab, Department of Ecology, Evolution and Behavior,*

*Alexander Silberman Institute of Life Sciences, Faculty of Science,
The Hebrew University of Jerusalem, Jerusalem 91904, Israel*

The presence of erratic or unstable paths in standard kinetic Monte Carlo simulations significantly undermines the accurate simulation and sampling of transition pathways. While typically reliable methods, such as the Gillespie algorithm, are employed to simulate such paths, they encounter challenges in efficiently identifying rare events due to their sequential nature and reliance on exact Monte Carlo sampling. In contrast, the weighted ensemble method effectively samples rare events and accelerates the exploration of complex reaction pathways by distributing computational resources among multiple replicas, where each replica is assigned a weight reflecting its importance, and evolves independently from the others. Here, we implement the highly efficient and robust weighted ensemble method to model susceptible-infected-susceptible (SIS) dynamics on large heterogeneous population networks. In particular, we explore the interplay between stochasticity and contact heterogeneity which gives rise to large fluctuations, leading to extinction (spontaneous clearance of infection). By studying a wide variety of networks characterized by fat-tailed degree distributions, we are able to compute the mean time to extinction as function of the various network and epidemic parameters. Importantly, this method allows exploring previously-inaccessible parameter regimes.

I. INTRODUCTION

Compartmental models are widely used in epidemiology for understanding the dynamics of infectious diseases within populations, aiding in the analysis of transmission patterns, disease prevalence, and the effectiveness of intervention strategies [1–8]. The crux of these models is to provide a structured framework to analyze complex interactions between various compartments representing different disease states, such as susceptible and infected individuals. Recently, compartmental models have played a key role in understanding the transmission of SARS-CoV-2 and informing public health strategies like vaccination, social distancing, and travel restrictions to mitigate the COVID-19 pandemic [9, 10]. Apart from epidemiology, such models have broad applications, e.g., in reliability engineering, election result forecasting, and the spread of computer viruses [11–13]. One of the simplest compartmental models is the Susceptible-Infected-Susceptible (SIS) model, which is widely used for modeling endemic states, where the disease persists beyond the initial number of infected individuals for an extended period, see e.g. [2, 3, 5–7, 14–16]. Amongst others, the SIS model effectively describes the dynamics of diseases such as influenza, the common cold, tuberculosis, and sexually transmitted infections like chlamydia and syphilis [5].

In the SIS model, a population is divided into two distinct groups, where individuals are either susceptible (S) to the infection or currently infected (I). Infected individuals may recover and revert to a susceptible state through treatment or natural recovery, while susceptible individuals can contract the disease upon contact with infected individuals. As long as the basic reproduction number R_0 is larger than 1 (see below), the model exhibits a stable endemic solution in which the disease persists within the population, as well as an unstable absorbing solu-

tion leading to disease extinction [1, 8]. However, demographic stochasticity, inherent in finite-size populations, ultimately drives the system from the stable to the unstable states via a rare large deviation [17–20]. Notably, despite their key role in determining the clearance probability, these large deviations are composed of a large number of sequential recovery events, rendering them challenging to observe using standard numerical methods.

In simple scenarios, there exists accurate analytical approaches that allow calculating the transition rates of such rare events, using semi-classical approximations of the pertinent master equations [21, 22]. These scenarios include a well-mixed, or *homogeneous* setting, where each individual interacts with an equal number of neighbors [18–20]. Recently, more realistic, *heterogeneous* scenarios were analytically studied; yet, analytical closed-form solutions are constrained to regimes where heterogeneity is weak or specific [23–26], or to regimes close to the bifurcation limit of the SIS model [27].

To overcome the analytical challenges, numerical methods are often employed to study rare events, with kinetic Monte Carlo (KMC) being the most common [28–31]. KMC simulations are powerful tools for studying the dynamics of complex systems across diverse scientific domains, spanning from semiconductor materials to epidemiology [8, 32]. The method employs stochastic sampling to model the time evolution of systems characterized by discrete events and transitions [28, 29]. Yet, the stochastic nature of KMC simulations requires performing a large number of realizations, each comprising numerous simulation steps, to achieve adequate statistics, leading to high computational costs [33]. KMC simulations may also encounter sampling inefficiency, thus facing challenges in effectively exploring high-dimensional phase spaces in heterogeneous environments [34].

As an alternative approach, a numerical solution to

the underlying set of time-dependent master equations can be found, which yields the probability distribution of finding a specific number of individuals in each state (susceptible or infectious) [35]. However, the computational efficiency of this method surpasses that of KMC only for low-dimensional systems [26, 35]. To overcome the exponential surge in runtime, as the system's dimension increases, in the limit of large population sizes, one can use semi-classical approximation schemes to transform the set of master equations to a set of Hamilton's equations, whose number increases linearly with the system's dimensions [19–21]. Nevertheless, these numerical schemes provide only limited accuracy, and are extremely sensitive to the initial conditions, rendering them as less practical in realistic, multi-dimensional cases.

In contrast, the weighted ensemble (WE) method offers an efficient approach for identifying and sampling rare events. By distributing computational resources among multiple replicas and adjusting weights dynamically, the WE method accelerates the exploration of complex reaction pathways, making it particularly suitable for studying rare events in dynamical systems [36]. Previously, this method was successfully applied for ecological, biological and chemical models with substantial computational benefit over "brute-force" methods [37–39]. Here we implement the WE method on large-population networks obeying the dynamics of the SIS model, and show that the method is highly effective in identifying extremely rare transitions from the endemic to the extinction states, for very large populations. Importantly, exploring large networks allows to accurately study a wide variety of real-world network topologies with varying heterogeneity strength, exhibiting fat-tailed distribution patterns, such as observed, e.g., in social networks, citation networks, and biological networks [2, 3, 40–44].

In this work we demonstrate the applicability and computational advantages of the WE method compared to "brute force" methods in studying rare events on population networks. We do so by exploring large networks with fat-tailed degree distributions, previously inaccessible due to the computational resources required. The WE method is shown to be vastly superior over previous methods, enabling the exploration of the SIS model in large population networks. In particular, we find that fat-tailed degree distributions significantly impact the mean time to extinction (MTE), and disease lifetime.

The paper is organized as follows. In Sec. II we present the theoretical model and known results for the MTE for simple network topologies, weak heterogeneity, and close to the bifurcation. In Sec. III we present the numerical algorithm we used and the obtained results. Finally in Sec. IV we conclude and present future directions.

II. THEORETICAL FORMULATION

We formulate the SIS model in a topologically heterogeneous network, where nodes represent individuals of

an isolated population of size N , each capable of being in either a susceptible (S) or infected (I) state [45, 46]. The network's topology is represented by an adjacency matrix \mathbf{A} , in which the elements indicate links between nodes, such that $A_{ij} = 1$ if nodes i and j are connected and 0 otherwise. Individuals can transition from being susceptible to infected only through links, representing potential interactions between individuals, and from infected to susceptible via spontaneous recovery. We define β as the infection rate, attributed to each link, and γ as the recovery rate, associated with each node.

In order to describe the dynamics in a rigorously amenable manner, we work under the annealed network approximation [8], which is basically a mean-field approximation over an ensemble of networks. For convenience, we partition nodes into groups based on their degree k , with each group having rates

$$I_k \xrightarrow{W_k^+(\mathbf{I})} I_k + 1, \quad I_k \xrightarrow{W_k^-(\mathbf{I})} I_k - 1. \quad (1)$$

Here, $W_k^+(\mathbf{I})$ and $W_k^-(\mathbf{I})$ denote the infection and recovery rates, respectively, while I_k is the number of infected individuals in group k , having degree k . While the recovery rate satisfies $W_k^-(\mathbf{I}) = \gamma I_k$, the node's infection rate depends on interactions with its neighbors. Under the annealed network approximation one may replace the adjacency matrix \mathbf{A} with its expectation value $\langle \mathbf{A} \rangle$ of an ensemble of networks [8], which for uncorrelated networks, satisfies: $\langle A_{ij} \rangle = k_i k_j / (N \langle k \rangle)$. Here k_i and k_j are the degrees of nodes i and j while $\langle k \rangle$ is the average degree. Let us assume that the network degree distribution is given by $p(k)$ and that there are N_k nodes of degree k , such that $\sum_k N_k = N$, and $N_k = N p(k)$. As a result, the infection rate satisfies

$$W_k^+(\mathbf{I}) = \beta k (N_k - I_k) \sum_{k'} \frac{k' I_{k'}}{N \langle k \rangle}, \quad (2)$$

where $1 \leq k \leq k_{\max}$ and k_{\max} is the maximal degree.

Given the network's degree distribution, $p(k)$, one can define the so-called basic reproduction number as

$$R_0 = \frac{\beta \langle k \rangle}{\gamma \langle k^2 \rangle}, \quad (3)$$

where here and henceforth $\langle k^i \rangle$ is the i -th moment of the distribution $p(k)$. As long as $R_0 > 1$, a nontrivial endemic state $I^* > 0$ prevails [2, 3]. In the deterministic limit, i.e. in the limit of an infinite population size and in the absence of noise, this endemic state is a stable fixed point, and the system remain there forever. As R_0 decreases and crosses the value of 1, a bifurcation occurs such that the endemic fixed point disappears. Thus, for $R_0 \leq 1$, disease extinction occurs deterministically. Yet, even for $R_0 > 1$ disease extinction can occur, but in this case it is driven by demographic noise. In order to take this noise into account, instead of dealing with a set of differential equations for the number of infected

individuals on degree- k nodes, we write down a set of coupled master equations for the joint probability, $P(\mathbf{I}, t)$, to find $\mathbf{I} = \{I_1, \dots, I_{k_{\max}}\}$ infected individuals on the different node degrees. Using the infection and recovery rates from above, the evolution equation for $P(\mathbf{I}, t)$ reads:

$$\frac{\partial P(\mathbf{I}, t)}{\partial t} = \sum_{k=1}^{k_{\max}} [W_k^-(I_k + 1)P(\mathbf{I} + \mathbf{1}_k, t) - W_k^-(I_k)P(\mathbf{I}, t) + W_k^+(I_k - 1)P(\mathbf{I} - \mathbf{1}_k, t) - W_k^+(I_k)P(\mathbf{I}, t)]. \quad (4)$$

Here, $\mathbf{I} \rightarrow \mathbf{I} \pm \mathbf{1}_j$ denotes an increase or decrease by one of group I_j [21].

While this master equation set is generally unsolvable for arbitrary degree distributions, one can proceed analytically in the limit of large population networks, $N \gg 1$. Here, the system enters a long lived metastable endemic state prior to disease extinction. This probability of being in this long-lived state slowly decays in time while simultaneously the extinction probability grows. To compute the MTE within exponential accuracy one can use the Wentzel-Kramers-Brillouin (WKB) approximation, which allows transferring Eq. (4) into a set of Hamilton's equations, whose solution provides the MTE up to exponential accuracy, in the form $T_{ext} \sim e^{NS}$, where S is called the action barrier to extinction [19–22, 27].

While the analytical treatment for general degree distributions can be found in [27], for completeness we provide the calculation in the simplest setting of a homogeneous population network, called a random regular network, where each node has degree $\langle k \rangle = k_0$. Here, the network's degree distribution satisfies $p(k) = \delta_{k, k_0}$, and as a result, the sum in Eq. (4) contains a single term, where the infection and recovery rates are, respectively: $W^+(I) = (\beta k_0/N)I(N - I)$ and $W^- = \gamma I$. Using the WKB method or other asymptotic expansions, the MTE has been shown to satisfy in the leading order [20, 47]:

$$T_{ext} \sim e^{NS}, \quad S = \ln(R_0) + 1/R_0 - 1, \quad (5)$$

where here $R_0 = \beta k_0/\gamma$.

The action barrier has also been computed for heterogeneous networks, but only in various parameter regimes, which give rise to an additional small parameter allowing to significantly reduce the dimensionality of the master equation set (4). Such is the scenario close to bifurcation, characterized by $R_0 - 1 \ll 1$. Here, the action barrier was analytically found to satisfy [27]

$$S = \frac{\langle k^2 \rangle^3}{2 \langle k^3 \rangle^2} (R_0 - 1)^2 + \mathcal{O}(R_0 - 1)^3. \quad (6)$$

Notably, in the limit of $R_0 - 1 \ll 1$, the action in Eq. (5) becomes $S \simeq (1/2)(R_0 - 1)^2$, which coincides with Eq. (6) for a homogeneous network.

More recently, the action barrier for heterogeneous networks with weak heterogeneity, and for arbitrary R_0 , has

been shown to satisfy [25]:

$$S = \mathcal{S}_0 - f(R_0)\epsilon^2 + \mathcal{O}(\epsilon)^3$$

$$f(R_0) = \frac{(R_0 - 1)(1 - 12R_0 + 3R_0^2) + 8R_0^2 \ln(R_0)}{4R_0^3}. \quad (7)$$

Here, \mathcal{S}_0 is the result for homogeneous network [Eq. (5)], and $\epsilon = \sigma/\langle k \rangle$ is the distribution's coefficient of variation ("strength" of the network heterogeneity), with σ being the distribution's standard deviation. Notably, Eq. (7) holds for weak heterogeneity, i.e., $\epsilon \ll 1$ [25].

However, computing the MTE for networks with an arbitrary topology, far from bifurcation, is analytically unfeasible. Thus, dealing with realistic scenarios necessitates using numerical schemes for determining the action barrier. In the next section we detail the numerical algorithm we have used to implement the KMC and WE simulations on population networks.

III. NUMERICAL SIMULATIONS

A. Methodology

To generate the network's topology we employ the configuration model that ensures no correlations between node degrees [48]. The random networks are characterized by their degree distribution $p(k)$, whose average and coefficient of variation, are given by $\langle k \rangle$ and ϵ , respectively. However, even among networks with an identical degree distribution, the adjacency matrix \mathbf{A} may vary. To address this variability, we generate multiple network realizations, compute the MTE for each realization, and average the results across all networks (see below). Furthermore, in all our comparisons between different networks, we kept the distance from the threshold R_0 constant, ensuring that the stability of the disease-free (extinct) state remains unchanged. However, as the network topology varies, the distance from the threshold changes as well. Thus, to maintain the same basic reproduction number across different networks, see Eq. (3), we adjust the ratio β/γ such that $\beta/\gamma = R_0/(1 + \epsilon^2)$.

To demonstrate the efficiency and usefulness of our algorithm, we took four different degree distributions, based on the gamma, beta, inverse Gaussian, and log-normal distributions, see Appendix for a detailed description. For $\epsilon \ll 1$, i.e., when the standard deviation is much smaller than the mean, these distributions exhibit a narrow peak and low variability, with a rapidly decaying tail. Conversely, when $\epsilon = \mathcal{O}(1)$, the variability increases and a fat tail on the right-hand side emerges. Here, accurate representation of these distributions requires large sample sizes due to the presence of numerous high-degree nodes in these networks. Therefore, simulations were conducted on networks comprising a large number of nodes to ensure a satisfactory degree distribution, as illustrated in Fig. 1 (see also Fig. S1).

The conventional method to simulate SIS dynamics involves the KMC approach, such as the Gillespie algo-

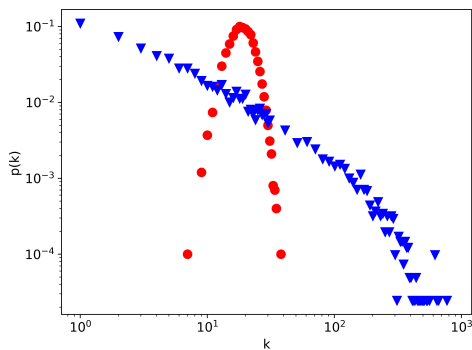


FIG. 1. Log-Log plot of the gamma degree distribution. Shown is $p(k)$ versus the degree k , for networks of size $N = 10^4$ with $\langle k \rangle = 20$. Circles and triangles denote networks with $\epsilon = 0.2$ and $\epsilon = 3.0$, respectively.

rithm [28–31]. Here, initially, a subset of nodes is randomly designated as infected, while the rest are labeled as susceptible. Transitions between states occur at exponentially distributed waiting times, where the time until the next reaction is stochastically determined based on the infection and recovery rates. We define the stochastic Gillespie time step between reactions as τ_G , and iteratively simulate these steps until the network reaches extinction. Due to the stochastic nature of the transition events, the network extinction times follow an exponential distribution. Hence, the network’s MTE and its confidence bounds are derived from fitting simulated extinction times to an exponential distribution. The overall MTE is obtained by averaging across several networks, while the standard deviation of the confidence bounds provides the MTE’s error bars. However, this simulation method is inherently slow, since accurately fitting the simulated extinction times to an exponential distribution necessitates a substantial number of realizations to capture the statistical properties. Furthermore, the method samples the phase space with computational time that is inversely proportional to the probability to be in a given state, resulting in a significant computational effort that is not necessarily concentrated on the rare event regions.

In contrast, the WE method involves simulating multiple realizations of the system simultaneously, each assigned weights contingent on their current state [36, 38, 49]. These weights are dynamically pruned to facilitate efficient exploration of the phase space by channeling computational resources towards the most relevant realizations. To determine the latter, the phase space is partitioned into bins, designating distinct regions of the system’s potential states. Bins are interactively chosen (on the fly), where regions close to extinction are set to include more instances, as detailed below (see also [50]).

We begin by initially dividing the phase space into two bins: one for states where the overall infected density exceeds I^* and one for those states with a lower density, where $I^* = 1 - 1/R_0$ is the endemic state in a well-mixed setting. Within each bin, m copies of a network are generated, with a fraction of randomly se-

lected infected nodes (seeds). Each realization is assigned a weight, representing its relative importance; initially, all realizations are assigned a weight of $1/(2m)$. Subsequently, the dynamics of each realization are simulated by Gillespie time steps until time τ_{WE} , which satisfies: $\tau_G \ll \tau_{WE} \ll T_{ext}$. At each WE step, i.e., upon reaching time τ_{WE} , the weight of those simulations that have undergone extinction, referred to as the extinction flux, is recorded. The surviving simulations undergo a resampling process, which entails the following: if a realization explores a new state with fewer infected individuals than previously recorded during each WE step, the bin closest to the extinction state is split at the new state, and the realization is replicated in the new (lowest) bin m times. For the remaining bins, for those with fewer than m realizations, the bin’s highest-weight realizations are iteratively split, until the bin contains m realizations. This splitting involves replicating the realization and dividing its weight equally. For bins with more than m realizations, randomly chosen subset(s) of low-weight realizations are combined such that m realizations remain in the bin. The combination of a subset includes choosing a single realization with probability proportional to its weight, and assigning the chosen realization’s weight as that of the total subset. The resampling process ends with each bin containing m weighted realizations. This WE step is performed M times, and the MTE satisfies:

$$T_{ext} = \frac{\tau_{WE}}{\frac{1}{M} \sum_{j=1}^M \phi_j}, \quad (8)$$

where ϕ_j represents the extinction flux at WE step j .

Two sources of uncertainty contribute in determining the overall error in the MTE: (i) stochastic nature of the WE method, which produces different results for the same network, and (ii) variability due to different network realizations. To assess the former, we ran WE simulation with a varying number of bins, realizations per bin, and resampling times. The standard deviation of these results served as the network confidence bounds. To assess the latter, we applied the WE method on multiple network realizations. The mean over all networks provided the overall MTE, while the standard deviation of the confidence bounds provided the MTE’s error bars.

In Fig. 2 we compare the runtimes of the KMC and WE methods. Here and in all other figures, the symbol size represents the maximal error bar. One can see that while the KMC scales exponentially with N , the WE method is significantly faster, scaling linearly with N ; e.g., if for $N = 10^3$ the runtimes were equal, for $N = 10^4$, the WE method out-competes the KMC by a factor of $\sim 10^4$. In Fig. 2 inset we also compare the MTE results of the two methods, confirming the WE method’s accuracy.

B. Results

We employed the WE method to compute the MTE for four different networks, each with a different degree dis-

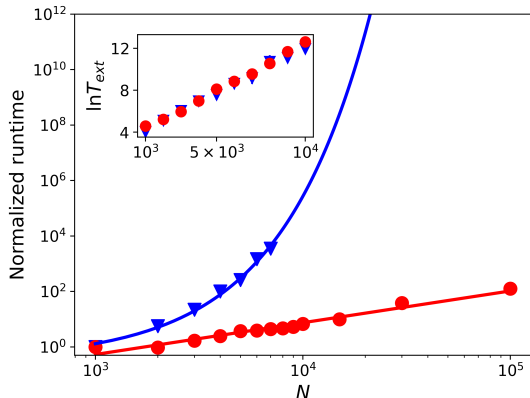


FIG. 2. A log-log plot of the runtime to obtain the MTE for each of the methods, versus the population size, N , normalized by the runtime at $N = 10^3$, for a gamma-distributed network. Here $\langle k \rangle = 10$, $\epsilon = 3.0$, and $R_0 = 1.3$. The triangles and circles represent the KMC and WE methods, respectively. The KMC scales exponentially with N (blue line – exponential fit), while the WE method scales linearly with N (red line – linear fit). The inset displays the logarithm of the MTE as a function of N , with circles and triangles representing the results of the KMC and WE methods, respectively, for the same parameters as in the main figure. Circles denote WE simulations results, while triangles denote KMC results.

tribution. Results for the gamma distribution are shown in Fig. 2, while results for the inverse-Gaussian, beta and log-normal distributions as a function of population size are shown in Fig. 3. Since we expect the MTE to have the following scaling: $T_{exp} \simeq A N^\alpha e^{NS}$ [19, 27], we have fitted the logarithm of the MTE to a linear function of N with logarithmic corrections. First of all, the WE method allows simulating huge networks of size $N = 10^5$ and more, which is well beyond the capabilities of the KMC method. Second, the scaling of the MTE with N holds for heterogeneous networks as well – here we have taken the COV ϵ to be very high, and still the simple formula, which was developed for the well-mixed case, qualitatively holds. Third, even though there is an offset between networks, one can see that the logarithmic slopes are similar across networks with similar degree distributions: identical mean and COV.

The impact of the coefficient of variation on the MTE is shown in Fig. 4, where the MTE is plotted against the square of the coefficient of variation. Notably, and as also seen in Fig. 3, the WE method allows us to obtain very long extinction times (here, up to 10^{130}), well beyond the capabilities of the KMC method. Our results indicate that the MTE strongly decreases with increasing ϵ ; namely, as heterogeneity increases, disease clearance becomes more and more likely, even for huge networks. For $\epsilon^2 = 8$ (highly skewed networks, see inset), the MTE drops dramatically. One can conjecture that the action barrier multiplying N in the exponent, see Eq. (5), vanishes as ϵ increases. This can be explained in a straight-

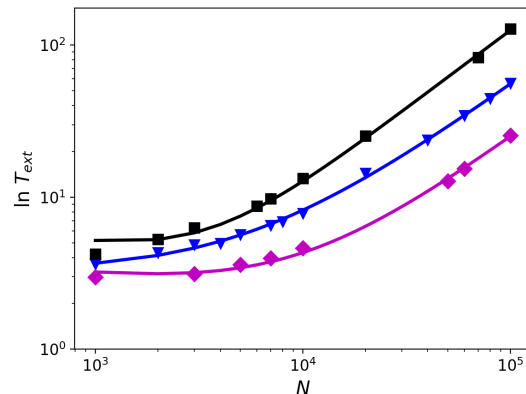


FIG. 3. Log-Log plot of the logarithm of MTE versus the population size, N , for networks with inverse-Gaussian (triangles), beta (squares) and log-normal (diamonds) degree distributions. Here, $\langle k \rangle = 10$, $\epsilon = 3.0$, and $R_0 = 1.3$. Solid lines depict linear fits with logarithmic corrections, see text.

forward manner: as the COV increases, there are more and more high-degree hubs. Once these recover, their neighbors' infection rate decreases which effectively decreases R_0 , making extinction more likely.

For weak heterogeneity we also compared our numerical results in Fig. 4 to previous analytical results obtained for heterogeneous networks with weak heterogeneity, see Eq. (7) [25]. Notably, the WE method allows to simulate huge networks with varying heterogeneity, and allows to plot the dependence of the MTE on ϵ for a wide range of COVs, which was inaccessible using the KMC method. Interestingly, given a network size, when heterogeneity is weak, the results for the MTE depend only on the mean and COV of the degree distribution, and are independent on its higher moments, as predicted by [25]. However, as ϵ increases, the different network results depart from each other, as they are no longer independent on the higher moments of the degree distribution, see inset of Fig. 4.

While the network size and COV play a crucial role in determining the MTE, other parameters may also be key in determining the extinction dynamics. Such is the basic reproduction number R_0 . In Fig. 5, the natural logarithm of the MTE is plotted as a function of R_0 for networks with different degree distributions but with the same mean degree and COV. First of all, as expected, the figure shows a dramatic increase in the MTE as R_0 increases, with a huge variability across networks for larger values of R_0 . Since we demand that the first two moments of the networks be identical, the variability here probably originates from the difference in the skewness of the networks, which strongly impacts rare events. The inset of Fig. 5 shows the MTEs close to bifurcation, where $R_0 - 1 \ll 1$. Here we find a good agreement between our numerical results and results found for arbitrary heterogeneous networks close to bifurcation, see Eq. (6) [27]. Notably, the significant differences across networks with the same mean and COV, emphasize the need for reliable

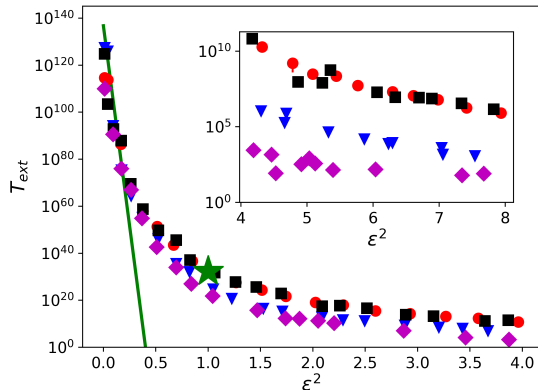


FIG. 4. The MTE versus COV squared, ϵ^2 , for networks with gamma (circles), inverse-Gaussian (triangles), beta (squares) and log-normal (diamonds) degree distributions. Here, $N = 10^4$, $\langle k \rangle = 20$, and $R_0 = 1.3$. The star denotes the MTE for a network with exponential degree distribution, with $\epsilon = 1$, while the solid line represents the analytical prediction for weak heterogeneity [Eq. (7)]. Inset shows the large- ϵ regime where the results for the various networks depart.

and fast numerical schemes, such as the WE method, to account for the complex interplay between topological and dynamical features.

IV. DISCUSSION

We have studied the long-time dynamics and disease extinction in the realm of the SIS model of epidemics using the so-called weighted-ensemble (WE) method. In most previous works, the SIS dynamics on population networks has been analyzed using the “brute-force” Gillespie kinetic Monte-Carlo (KMC) algorithm. This algorithm is excellent, when one is interested in simulating short time scales related to the emergence of the endemic state and its relaxation dynamics, or to compute the extinction dynamics on small networks. However, the algorithm becomes infeasible computationally for large heterogeneous networks. Naturally, the sequential nature of the KMC prevents the study of rare events such as disease extinction, as the computational time required grows exponentially with the system size. Furthermore, when heterogeneity increases, the huge variability between node degrees makes standard KMC algorithms less efficient, as time steps may become vanishingly small.

The WE method, which we have introduced here to study rare events on population networks, efficiently explores reaction pathways by generating multiple replicas. As the simulation progresses, replicas that are close to extinction are allocated more computational resources, while others are discarded, thereby enabling us to study large heterogeneous population networks that were previously inaccessible with KMC methods. After demonstrating an equivalence between the KMC and WE meth-

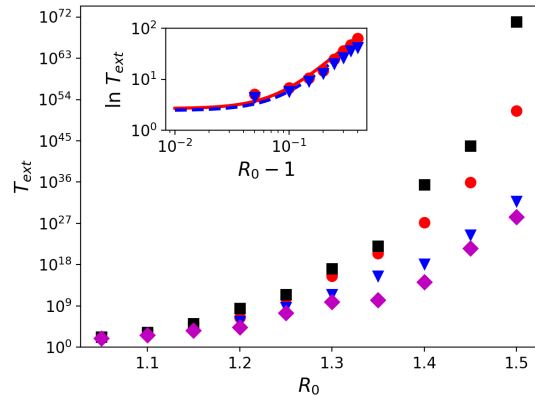


FIG. 5. The MTE versus the basic reproduction number, R_0 , for networks with gamma (circles), inverse-Gaussian (triangles), beta (squares) and log-normal (diamonds) degree distributions. Here $N = 10^4$, $\langle k \rangle = 20$, and $\epsilon = 1.5$. Inset shows a log-log plot of $\ln T_{ext}$ versus $R_0 - 1$ for gamma- (circles) and inverse-Gaussian-distributed (triangles) networks. Here, the solid and dashed lines depict the analytical prediction, Eq. (6), for these networks.

ods and showing that the runtime of the latter scales linearly with the system’s size, we studied the dependence of the mean time to extinction (MTE) on three main features: the network’s size N , its coefficient of variation ϵ , and the basic reproduction number R_0 . We have found that the dependence on N in strongly heterogeneous networks is qualitatively similar to that of well-mixed systems. We have also found that increasing heterogeneity drastically decreases the disease lifetime. Finally, we have shown that increasing R_0 causes a surge in the MTE and span across networks with similar characteristics. In addition, we have managed to asymptotically corroborate our results against known analytical results in the limits of weak heterogeneity and close to bifurcation.

While we have focused on random networks, with no degree correlations between nearest neighbors, the WE method can also be used to study assortative networks. These are characterized by the tendency of high-degree nodes to be connected to other high-degree nodes, and vice versa; as a result they tend to percolate more easily, forming a giant component that contains a significant fraction of the entire network’s nodes [51, 52]. It has been recently shown that correlation between neighboring nodes can alter the outbreak threshold [46, 53] and change the outbreak size distribution’s characteristics [54]. Yet, the study of rare events on assortative networks requires large populations sizes, to overcome finite size effects. Thus, the WE method implemented here is ideal for studying the interplay between network heterogeneity and assortativity. Since the latter is prevalent in many types of networks such as social, technological, and biological networks [8, 51, 52], the WE method can play a key role in future studies of complex networks.

V. ACKNOWLEDGMENTS

EK and MA acknowledge support from ISF grant 531/20.

APPENDIX: DEGREE DISTRIBUTIONS

Here, we outline the definitions of the degree distributions employed in generating networks via the configuration model: gamma, beta, inverse-Gaussian (Wald), and log-normal distribution; see Figs. 1 and S1. For each we specify the probability density function (PDF) along with its defining parameters, which are then tied to the mean degree, $\langle k \rangle$, and coefficient of variation, ϵ .

A. Gamma-distribution

The PDF of a gamma distribution with a shape parameter $\kappa > 0$ and scale parameter $\theta > 0$ is given by,

$$p(x; \kappa, \theta) = \frac{1}{\Gamma(\kappa)\theta^\kappa} x^{\kappa-1} e^{-\frac{x}{\theta}}, \quad x \geq 0, \quad (\text{A1})$$

where $\Gamma(\kappa)$ is the gamma function. Demanding that the mean and standard deviation of the gamma distribution are $\langle k \rangle$ and $\epsilon \langle k \rangle$, respectively, one has:

$$\theta = \epsilon^2 \langle k \rangle, \quad \kappa = \frac{1}{\epsilon^2} \iff \langle k \rangle = \kappa \theta, \quad \epsilon = \frac{1}{\sqrt{\kappa}}. \quad (\text{A2})$$

Here, to obtain a fat-tailed distribution, one must have $\kappa \lesssim 1$. If one is interested in having both large mean and large COV, one has to choose $\theta^{-1} \ll \kappa \lesssim 1$, which yields distributions such as shown in blue in Fig. S1.

B. Beta-distribution

The beta distribution's PDF is represented as follows:

$$p(x; \alpha, \beta) = \frac{1}{B(\alpha, \beta)} x^{\alpha-1} (1-x)^{\beta-1}, \quad 0 \leq x \leq 1 \quad (\text{A3})$$

Here, α and β denote the shape parameters, and $B(\alpha, \beta)$ is the beta function. Since the beta distribution has compact support, we demand that the mean and standard deviation of the beta distribution are $\langle k \rangle/N$ and $\epsilon \langle k \rangle$, respectively. In the limit of $N \gg \langle k \rangle$ we find:

$$\alpha \simeq \frac{1}{\epsilon^2}, \quad \beta \simeq \frac{N}{\langle k \rangle \epsilon^2} \iff \langle k \rangle \simeq \frac{N\alpha}{\beta}, \quad \epsilon \simeq \frac{1}{\sqrt{\alpha}}. \quad (\text{A4})$$

Here, to obtain a fat-tailed distribution, one must have $\alpha \lesssim 1$. If one is interested in having both large mean and large COV, one has to choose $\beta/N \ll \alpha \lesssim 1$, which yields distributions such as shown in blue in Fig. S1.

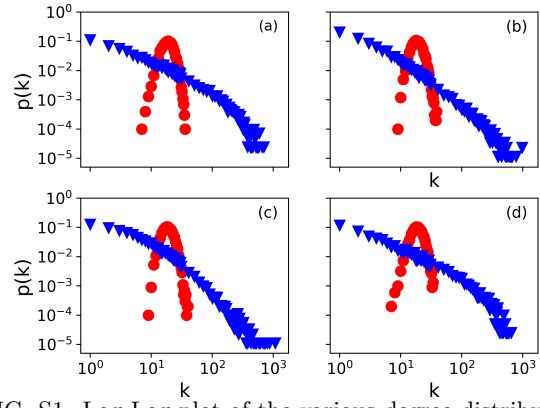


FIG. S1. Log-Log plot of the various degree distributions we have used, for networks of size $N = 10^4$ and an average degree of $\langle k \rangle = 20$. The distributions are Gamma (Panel a), Beta (panel b), log-normal (panel c), and inverse-Gaussian (panel d). In each panel circles denote networks with $\epsilon = 0.2$, while triangles denote networks with $\epsilon = 3.0$.

C. Wald distribution

The inverse Gaussian distribution, also known as the Wald distribution, has a PDF given by:

$$p(x; \mu, \lambda) = \sqrt{\frac{\lambda}{2\pi x^3}} \exp\left[-\frac{\lambda(x-\mu)^2}{2\mu^2 x}\right], \quad x > 0. \quad (\text{A5})$$

Here $\mu > 0$ is the mean and $\lambda > 0$ is the shape parameter. This distribution gives the time distribution of a Brownian particle with positive drift to reach a fixed positive level. Comparing with the network distribution, we find:

$$\mu = \langle k \rangle, \quad \lambda = \frac{\langle k \rangle}{\epsilon^2} \iff \langle k \rangle = \mu, \quad \epsilon = \sqrt{\frac{\mu}{\lambda}}. \quad (\text{A6})$$

Here, to obtain a fat-tailed distribution and a large mean, one has to take a large μ value and $\lambda \lesssim \mu$, which yields distributions such as shown in blue in Fig. S1.

D. Log-normal distribution

Lastly, the log-normal distribution PDF reads,

$$p(x; \mu, \sigma) = \frac{1}{x\sigma\sqrt{2\pi}} \exp\left[-\frac{(\ln x - \mu)^2}{2\sigma^2}\right], \quad x > 0, \quad (\text{A7})$$

where μ represents the mean of the natural logarithm of the random variable x and σ is its standard deviation. Comparing with the network distribution, we find:

$$\begin{aligned} \mu &= -\frac{1}{2} \ln\left(\frac{1+\epsilon^2}{\langle k \rangle^2}\right), \quad \sigma^2 = \ln(1+\epsilon^2) \iff \\ \langle k \rangle &= e^{\mu + \frac{\sigma^2}{2}}, \quad \epsilon = \sqrt{e^{\sigma^2} - 1}. \end{aligned} \quad (\text{A8})$$

Here, to obtain a fat-tailed distribution with a large mean, one must have $\sigma \gtrsim 1$ and a large enough μ , such that $\mu + \sigma^2/2 \gg 1$, which yields distributions such as shown in blue in Fig. S1.

-
- [1] H. W. Hethcote, The mathematics of infectious diseases, *SIAM Review* **42**, 599 (2000).
- [2] R. Pastor-Satorras and A. Vespignani, Epidemic spreading in scale-free networks, *Phys. Rev. Lett.* **86** (2001).
- [3] R. Pastor-Satorras and A. Vespignani, Epidemic dynamics and endemic states in complex networks, *Phys. Rev. E* **63**, 066117 (2001).
- [4] R. Pastor-Satorras and A. Vespignani, Epidemic dynamics in finite size scale-free networks, *Phys. Rev. E* **65**, 035108 (2002).
- [5] M. J. Keeling and K. T. Eames, Networks and epidemic models, *Journal of the royal society interface* **2**, 295 (2005).
- [6] S. N. Dorogovtsev, A. V. Goltsev, and J. F. F. Mendes, Critical phenomena in complex networks, *Rev. Mod. Phys.* **80**, 1275 (2008).
- [7] M. J. Keeling and P. Rohani, *Modeling infectious diseases in humans and animals* (Princeton university press, 2011).
- [8] R. Pastor-Satorras, C. Castellano, P. Van Mieghem, and A. Vespignani, Epidemic processes in complex networks, *Rev. Mod. Phys.* **87** (2015).
- [9] M. Chinazzi, J. T. Davis, M. Ajelli, C. Gioannini, M. Litvinova, S. Merler, A. P. y Piontti, K. Mu, L. Rossi, K. Sun, C. Viboud, X. Xiong, H. Yu, M. E. Halloran, I. M. Longini, and A. Vespignani, The effect of travel restrictions on the spread of the 2019 novel coronavirus (covid-19) outbreak, *Science* **368** (2020).
- [10] Comparative cost-effectiveness of sars-cov-2 testing strategies in the usa: a modelling study, *The Lancet Public Health* **6**, e184 (2021).
- [11] B. Schäfer, M. Matthiae, X. Zhang, M. Rohden, M. Timme, and D. Witthaut, Escape routes, weak links, and desynchronization in fluctuation-driven networks, *Phys. Rev. E* **95** (2017).
- [12] A. Volkening, D. F. Linder, M. A. Porter, and G. A. Rempala, Forecasting elections using compartmental models of infection, *SIAM Review* **62**, 837 (2020).
- [13] J. Wierman and D. Marchette, Modeling computer virus prevalence with a susceptible-infected-susceptible model with reintroduction, *Computational Statistics and Data Analysis* **45** (2004).
- [14] C. Moore and M. E. Newman, Epidemics and percolation in small-world networks, *Physical Review E* **61**, 5678 (2000).
- [15] B. Karrer and M. E. Newman, Message passing approach for general epidemic models, *Physical Review E* **82**, 016101 (2010).
- [16] C. Castellano and R. Pastor-Satorras, Relevance of backtracking paths in recurrent-state epidemic spreading on networks, *Phys. Rev. E* **98**, 052313 (2018).
- [17] A. Nold, Heterogeneity in disease-transmission modeling, *Mathematical Biosciences* **52** (1980).
- [18] O. Ovaskainen, The quasistationary distribution of the stochastic logistic model, *Journal of Applied Probability* **38** (2001).
- [19] M. Assaf and B. Meerson, Extinction of metastable stochastic populations, *Phys. Rev. E* **81** (2010).
- [20] M. Assaf and B. Meerson, WKB theory of large deviations in stochastic populations, *Journal of Physics A: Mathematical and Theoretical* **50** (2017).
- [21] M. I. Dykman, E. Mori, J. Ross, and P. M. Hunt, Large fluctuations and optimal paths in chemical kinetics, *The Journal of Chemical Physics* **100**, 5735 (1994).
- [22] M. I. Dykman, I. B. Schwartz, and A. S. Landsman, Disease extinction in the presence of random vaccination, *Physical review letters* **101** (2008).
- [23] D. Clancy, Persistence time of SIS infections in heterogeneous populations and networks, *J Math Biol* **77**, 545 (2018).
- [24] D. Clancy, Precise estimates of persistence time for sis infections in heterogeneous populations, *Bulletin of Mathematical Biology* **80**, 2871 (2018).
- [25] J. Hindes and M. Assaf, Degree dispersion increases the rate of rare events in population networks, *Phys. Rev. Lett.* **123**, 068301 (2019).
- [26] E. Korngut, J. Hindes, and M. Assaf, Susceptible-infected-susceptible model of disease extinction on heterogeneous directed population networks, *Phys. Rev. E* **106** (2022).
- [27] J. Hindes and I. B. Schwartz, Epidemic extinction and control in heterogeneous networks, *Phys. Rev. Lett.* **117** (2016).
- [28] D. T. Gillespie, A general method for numerically simulating the stochastic time evolution of coupled chemical reactions, *Journal of Computational Physics* **22** (1976).
- [29] D. T. Gillespie, Exact stochastic simulation of coupled chemical reactions, *The Journal of Physical Chemistry* **81**, 2340 (1977).
- [30] D. T. Gillespie, Stochastic simulation of chemical kinetics, *Annual Review of Physical Chemistry* **58** (2007).
- [31] P. G. Fennell, S. Melnik, and J. P. Gleeson, Limitations of discrete-time approaches to continuous-time contagion dynamics, *Phys. Rev. E* **94** (2016).
- [32] I. Martin-Bragado, R. Borges, J. P. Balbuena, and M. Jaraiz, Kinetic monte carlo simulation for semiconductor processing: A review, *Progress in Materials Science* **92**, 1 (2018).
- [33] S. Gómez, J. Gómez-Gardeñes, Y. Moreno, and A. Arenas, Nonperturbative heterogeneous mean-field approach to epidemic spreading in complex networks, *Phys. Rev. E* **84**, 036105 (2011).
- [34] B. S. Lindley and I. B. Schwartz, An iterative action minimizing method for computing optimal paths in stochastic dynamical systems, *Physica D: Nonlinear Phenomena* **255** (2013).
- [35] M. J. Keeling and J. V. Ross, On methods for studying stochastic disease dynamics, *J R Soc Interface* **5** (2008).
- [36] G. Huber and S. Kim, Weighted-ensemble brownian dynamics simulations for protein association reactions, *Biophysical Journal* **70**, 97 (1996).
- [37] R. M. Donovan, A. J. Sedgewick, J. R. Faeder, and D. M. Zuckerman, Efficient stochastic simulation of chemical kinetics networks using a weighted ensemble of trajectories, *The Journal of Chemical Physics* **139** (2013).
- [38] O. Vilks and M. Assaf, Extinction risk of a metapopulation under bistable local dynamics, *Phys. Rev. E* **101** (2020).
- [39] O. Vilks, M. Assaf, and B. Meerson, Fluctuations and first-passage properties of systems of brownian particles with reset, *Phys. Rev. E* **106**, 024117 (2022).

- [40] A. S. Novozhilov, On the spread of epidemics in a closed heterogeneous population, *Mathematical Biosciences* **215** (2008).
- [41] L. Muchnik, S. Pei, L. C. Parra, S. D. S. Reis, J. S. Andrade Jr, S. Havlin, and H. A. Makse, Origins of power-law degree distribution in the heterogeneity of human activity in social networks, *Scientific Reports* **3**, 1783 (2013).
- [42] M. Brzezinski, Power laws in citation distributions: evidence from scopus, *Scientometrics* **103**, 213 (2015).
- [43] B. Qu and H. Wang, Sis epidemic spreading with heterogeneous infection rates, *IEEE Transactions on Network Science and Engineering* **4** (2017).
- [44] J. Neipel, J. Bauermann, S. Bo, T. Harmon, and F. Jülicher, Power-law population heterogeneity governs epidemic waves, *PLOS ONE* **15** (2020).
- [45] N. Bailey, *The mathematical theory of infectious diseases* (griffin, london, 1975), ; jd murray, *Mathematical Biology* (1993).
- [46] S. Morita, Solvable epidemic model on degree-correlated networks, *Physica A: Statistical Mechanics and its Applications* **563** (2021).
- [47] Stochastic models of population extinction, *Trends in Ecology and Evolution* **25**, 643 (2010).
- [48] B. K. Fosdick, D. B. Larremore, J. Nishimura, and J. Ugander, Configuring random graph models with fixed degree sequences, *SIAM Review* **60**, 315 (2018).
- [49] D. J. Sharpe and D. J. Wales, Efficient and exact sampling of transition path ensembles on Markovian networks, *The Journal of Chemical Physics* **153** (2020).
- [50] Our codes for network generation and WE numerical simulations were carried out using python and c++, and are available upon request.
- [51] M. E. J. Newman, Assortative mixing in networks, *Phys. Rev. Lett.* **89** (2002).
- [52] M. E. J. Newman, Mixing patterns in networks, *Phys. Rev. E* **67**, 026126 (2003).
- [53] D. H. Silva, S. C. Ferreira, W. Cota, R. Pastor-Satorras, and C. Castellano, Spectral properties and the accuracy of mean-field approaches for epidemics on correlated power-law networks, *Phys. Rev. Res.* **1**, 033024 (2019).
- [54] A. Leibenzon and M. Assaf, Heterogeneity can markedly increase final outbreak size in the sir model of epidemics, *Physical Review Research* **6**, L012010 (2024).